

# In-process Monitoring during Stamping of Thin Plate: Propagation Characteristics of Ultrasonic Waves in Cylindrical Stamping Dies

Naoto Hagino,<sup>1\*</sup> Seiji Komiya,<sup>2</sup> Junichi Endou,<sup>2</sup> and Masao Ishihama<sup>3</sup>

<sup>1</sup>Department of Comprehensive Engineering, Kindai University Technical College,  
7-1 Kasugaoka, Nabari, Mie 518-0459, Japan

<sup>2</sup>Department of Vehicle System Engineering, Kanagawa Institute of Technology,  
1030 Shimo-ogino, Atsugi, Kanagawa 243-0292, Japan

<sup>3</sup>Engineering Research Institute, Kanagawa University, 3-27-1 Rokkakubashi,  
Kanagawa-ku, Yokohama, Kanagawa 221-8686, Japan

(Received March 1, 2019; accepted June 19, 2019)

**Keywords:** in-process monitoring, ultrasonic wave, sheet metal forming, stamping, FDTD method

A method of using ultrasonic waves to measure contact states between a workpiece and dies during stamping has been developed. The method is based on the fact that ultrasonic waves are reflected at the boundary of air gaps between a workpiece and a die. In our previous studies, the experimental and numerical analysis results for flat and V-shaped stamping dies show that the contact state can be monitored using ultrasonic waves. However, machine parts made by stamping consist of not only flat surfaces but also inclined or curved surfaces. When an ultrasonic wave is incident on an inclined or curved surface, modal conversion of the ultrasonic wave occurs. Thus, acoustic fields near the boundary surface become complicated. In this study, we investigate the reflection and transmission characteristics of ultrasonic waves at the contact surface between cylindrical stamping dies. The following results were obtained: (1) the reflection of ultrasonic waves was affected by the die shape but (2) when a thin metal plate was firmly attached to the stamping die, the transmitted waves were not greatly affected by the die shape.

## 1. Introduction

The servo press has high potential for producing high-precision mechanical parts. However, it is widely known that during stamping small gaps exist between the dies and the workpieces. These gaps are mainly caused by inadequate positioning accuracy of the workpieces and dies and by elastic deformation of the dies and press slide. The reason that the gaps are not removed during stamping is that the presses are not controlled by contact information as feedback signal. To achieve so-called net-shape forming, the die shape must be precisely copied to the workpiece. If the slide motion could be controlled by feeding back contact information, small gaps could be removed. It is thus necessary to develop methods of measuring the contact states between the workpiece and the die. The contact pressure between the tool and the workpiece can be

---

\*Corresponding author: e-mail: [hagino@kct.ac.jp](mailto:hagino@kct.ac.jp)  
<https://doi.org/10.18494/SAM.2019.2355>

measured by using ultrasonic waves,<sup>(1)</sup> and the contact area between a mirror surface and a regular surface can be estimated by using reflected waves.<sup>(2)</sup> Additionally, an ultrasonic method has been used to measure the contact states between a bearing and a bearing housing.<sup>(3)</sup> We have already proposed a method of using ultrasonic waves to measure the contact states between the workpiece and the die during stamping.<sup>(4–6)</sup> The reflected and transmitted wave heights could be used with this method to measure the contact states between the workpiece and the die. Additionally, we examined the propagation of ultrasonic waves near the boundary surface by nominal analysis.<sup>(7,8)</sup> The sound fields in stamping dies were solved by the finite-difference time-domain (FDTD) method. The results of this FDTD simulation enable the visualization of wave propagation, which could not be experimentally measured.<sup>(7–10)</sup> However, the actual products made by stamping have complicated shapes that consist of inclined or curved surfaces. When ultrasonic waves obliquely enter the workpiece, modal conversion of elastic waves occurs at the boundary between the surfaces of the workpiece and die. Therefore, the acoustic fields near the boundary are complicated. In this study, we investigate the reflection and transmission characteristics of ultrasonic waves at the contact surface between the workpiece and cylindrical stamping dies.

## 2. Principle of In-process Monitoring during Stamping

Figure 1 illustrates the propagation of ultrasonic waves at the boundary between two materials. The ultrasonic waves are transmitted into material 1 from an ultrasonic probe. The waves are either reflected or transmitted at the boundary between the surfaces of two materials. The ratio of waves reflected is called the sound pressure reflectance<sup>(1)</sup> and is given by

$$R_R = |(Z_1 - Z_2) / (Z_1 + Z_2)|, \quad (1)$$

where  $Z$  is the acoustic impedance and subscripts 1 and 2 correspond to materials 1 and 2. Here,  $Z$  is defined by

$$Z = \rho c l, \quad (2)$$

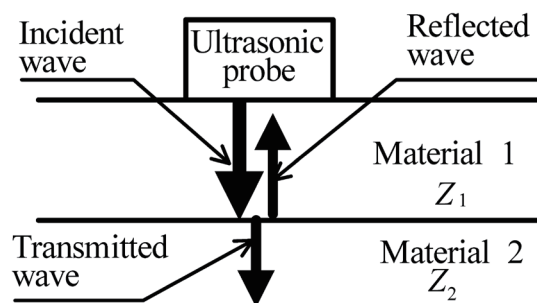


Fig. 1. Propagation of ultrasonic waves at boundary between different materials.

where  $\rho$  is the density and  $c_l$  is the acoustic velocity of the longitudinal elastic wave in the material.

If  $Z_2$  is far smaller than  $Z_1$ ,  $R_R$  is approximately one. For example, if materials 1 and 2 are steel and air, respectively,  $R_R$  is almost 1, which means that we should be able to measure the change in the gap between a workpiece and a die by using ultrasonic waves.

Figure 2 shows the procedure of in-process monitoring during stamping. When the press slide reaches the bottom dead center, the workpiece firmly attaches to the dies. Then, the reflected wave intensity decreases, and the intensity of the transmitted wave increases. The reflected wave height  $e_R$  and the transmitted wave height  $e_T$  are defined as indicated in Fig. 2. We have already established that the contact states can be measured by using these wave heights in cases of flat dies and V-shape dies. This method was applied to cylindrical dies.

### 3. Experimental Apparatus and Measurement Procedure

First, we examined the reflection characteristics when there was only the lower die. Figure 3 shows the experimental setup. The die radius was 20 mm, and the die material was S45C-JIS. Two probes were set on the lower die. Probe 1 was an ultrasonic wave transmitter. The ultrasonic waves incident on the die were from probe 1. When the ultrasonic waves reached the cylindrical die surface, they were reflected at this surface. The reflected waves diffused owing to the effect of the cylindrical die surface. To investigate the diffusion of ultrasonic waves, we measured the ultrasonic waves while moving probe 2 along the surface of the lower die. The dashed lines in Fig. 3 indicate ultrasonic wave paths.

We examined the reflection characteristics of ultrasonic waves at the boundary between a workpiece and dies (the upper and lower dies). Figure 4 shows the experimental setup for in-process monitoring using cylindrical dies. The ultrasonic waves were incident from probe 1,

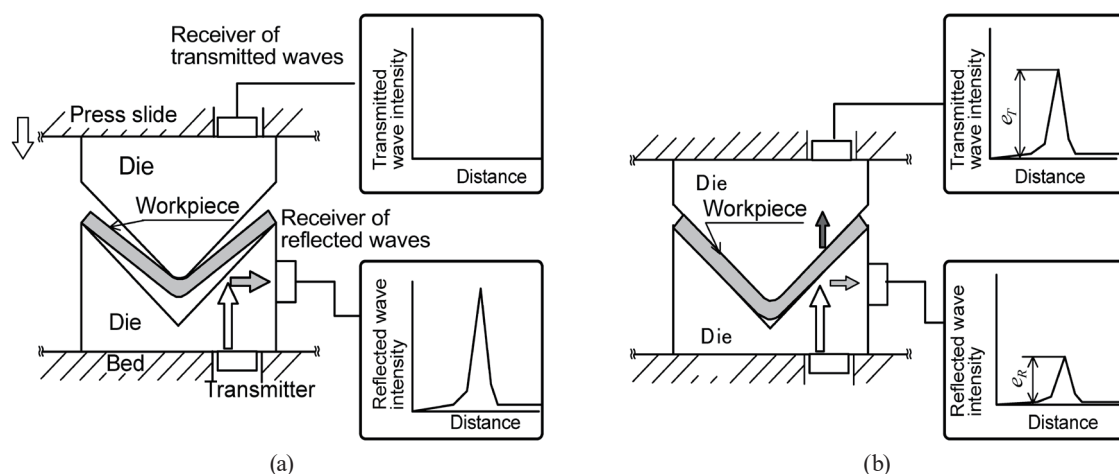


Fig. 2. Schematic of in-process monitoring during stamping. (a) Press slide before reaching bottom dead center. (b) Press slide reaches bottom dead center.

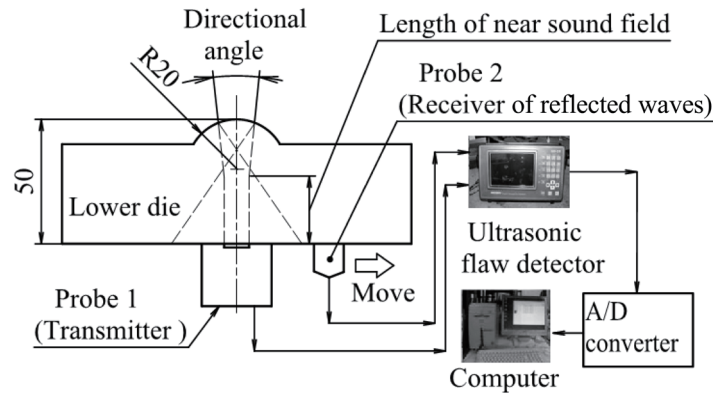


Fig. 3. Experimental setup for investigating reflection characteristics when there is only the lower die.

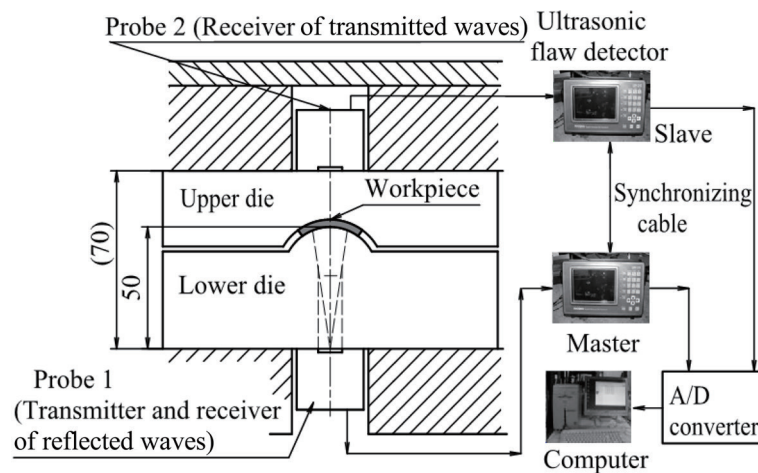


Fig. 4. Experimental setup with cylindrical dies.

which was set on the lower die. Probe 1 was both the transmitter and receiver. Probe 2, which was set on the upper die portion, received the transmitted waves. The die was loaded in the downward direction by a weight. The lower die height was 50 mm, and the total die height was 70 mm. The die material was S45C-JIS. An ultrasonic probe that emitted 5 MHz ultrasonic waves with 10 mm diameter oscillator was installed on the bottom of the lower die portion. The reflected wave height during loading was measured using an ultrasonic detector that was part of the same probe. The contact area between the  $800 \times 110 \text{ mm}^2$  workpiece and the die was  $800 \text{ mm}^2$ . The workpieces were 0.13 mm thick, and the workpiece material was aluminum.

#### 4. Experimental Results

First, we examined the reflection characteristics when using only the lower die of the apparatus. The experimental results are shown in Fig. 5. The measured wave height increased

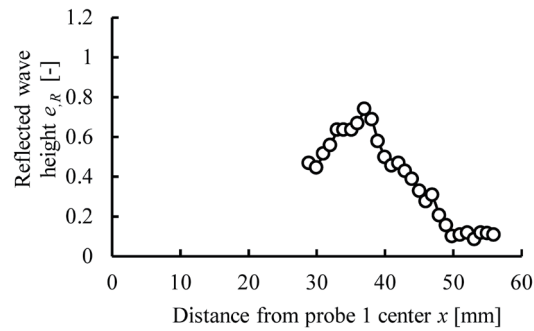


Fig. 5. Diffusion of ultrasonic waves at bottom surface of cylindrical die.

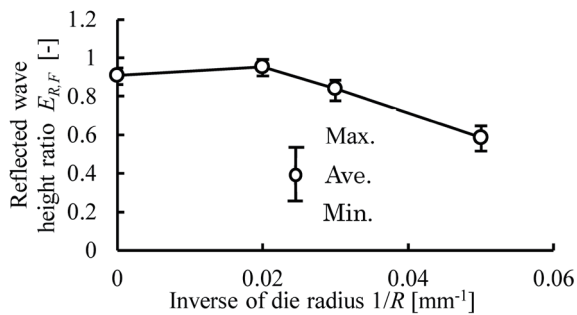


Fig. 6. Effect of die radius on reflected wave height ratio.

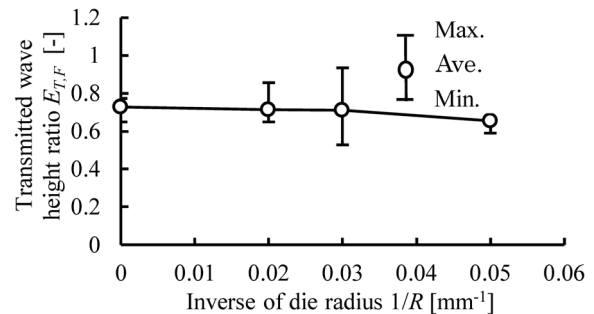


Fig. 7. Effect of die radius on transmitted wave height ratio.

with distance from the center of probe 1. The wave height peaked when  $x$  was approximately 37 mm. After that, the reflected wave height sharply decreased. The reflected wave height was not measured at 50 mm and above from the center of the transmitter. Therefore, it was found that the ultrasonic waves were reflected on the curved surface and were spread widely over the bottom surface of the die.

Figures 6 and 7 show the effect of die radius on the reflection and transmission characteristics of ultrasonic waves. In these figures, the horizontal axis shows the inverse of the die radius, and the vertical axis is the wave height ratio.  $E_{R,F}$  and  $E_{T,F}$  are defined as

$$E_{R,F} = e_R / e_{R,0}, \quad (3)$$

$$E_{T,F} = e_T / e_{R,0}, \quad (4)$$

where  $e_R$  and  $e_T$  are the reflected and transmitted wave heights, respectively, and  $e_{R,0}$  is the reflected wave height without a workpiece.  $1/R = 0 \text{ mm}^{-1}$  represents the case of a flat die.

The characteristics of reflected ultrasonic waves are greatly affected by the die radius. The reflected waves are concentrated at one point owing to the effect of the cylindrical die surface.

We believe that the incident angle of an incident wave to the contact surface continuously varies along the contact surface, as shown in Fig. 8. Therefore, if the receiver of reflected waves is installed in the vicinity of the focal spot, the amplified waves can be measured. However, if the receiver is outside the focal spot, the reflected wave intensity decreases, and it becomes difficult to measure the reflected waves. On the other hand, measuring reflected waves at the focal point, if possible, is effective. However, if the receiver of the reflected waves is outside the focal spot, it may be impossible to measure the contact state between the workpiece and the dies.

On the other hand, transmitted waves were less affected by the die radius. A transmitted wave is refracted at both contact surface 1 and contact surface 2, and the traveling direction of the transmitted wave is almost the same as that of the incident wave (Fig. 8). When the workpiece is a thin plate, the propagation path of ultrasonic waves through the workpiece is short. Hence, it is considered that the effect of the cylindrical surface is small. Thus, the receiver can measure transmitted waves without being affected by the shape of the dies during the stamping of the thin plate.

## 5. Numerical Analysis Results

As described in the previous section, the experimental results showed that the reflected waves are affected by the shape of the dies, whereas the transmitted waves are not greatly affected by the cylindrical dies. In this section, we investigated the reflection and transmission characteristics by numerical simulation.

The ultrasonic waves emitted from the ultrasonic transmitter propagate in the solid metal as elastic waves without plastic deformation. When sound fields in the  $y$ -direction are uniform, the fundamental equations for elastic waves in the solid metal are expressed by Eqs. (5) and (6). Equation (5) describes Hooke's law and Eq. (6) describes particle motion.<sup>(11)</sup> Here,  $c_{11}$ ,  $c_{33}$ ,  $c_{55}$ , and  $c_{13}$  are the components of a stiffness matrix. The materials used in this numerical analysis have isotropic elasticity, i.e.,  $c_{11} = c_{33}$  and  $c_{55} = (c_{11} - c_{13})/2$ .  $T_{xx}$  and  $T_{zz}$  are normal stresses, and  $T_{xz}$  is shear stress.  $\dot{u}$  and  $\dot{w}$  are the velocities in the  $x$ - and  $z$ -directions, respectively.

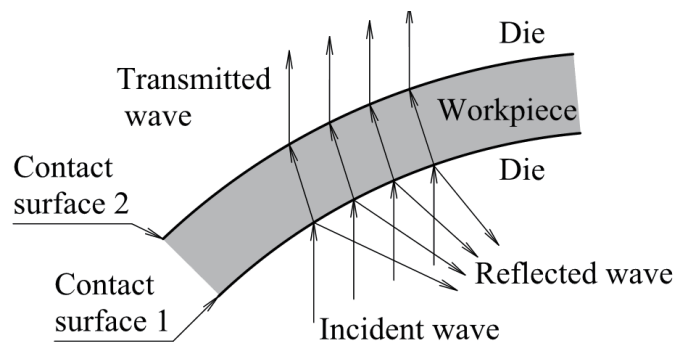


Fig. 8. Propagation direction of ultrasonic wave around contact surface between workpiece and cylindrical dies.

$$\frac{\partial}{\partial t} \begin{bmatrix} T_{xx} \\ T_{zz} \\ T_{xz} \end{bmatrix} = \begin{bmatrix} c_{11} & c_{13} & 0 \\ c_{13} & c_{33} & 0 \\ 0 & 0 & c_{55} \end{bmatrix} \begin{bmatrix} \frac{\partial \dot{u}}{\partial x} \\ \frac{\partial \dot{w}}{\partial z} \\ \frac{\partial \dot{u}}{\partial z} + \frac{\partial \dot{w}}{\partial x} \end{bmatrix} \quad (5)$$

$$\rho \frac{\partial}{\partial t} \begin{bmatrix} \dot{u} \\ \dot{w} \end{bmatrix} = \begin{bmatrix} \frac{\partial T_{xx}}{\partial x} + \frac{\partial T_{xz}}{\partial z} \\ \frac{\partial T_{zz}}{\partial z} + \frac{\partial T_{xz}}{\partial x} \end{bmatrix} \quad (6)$$

The vector of particle velocity<sup>(9–12)</sup> is represented as Eq. (7) by using the velocity potential

$$\dot{\mathbf{u}} = \text{grad } \Phi + \text{rot } \Psi, \quad (7)$$

where  $\Phi$  is the scalar velocity potential,  $\Psi = [\Psi_1, \Psi_2, \Psi_3]$  is the vector velocity potential, and  $\dot{\mathbf{u}} = [\dot{u}, \dot{v}, \dot{w}]$  is the vector of particle velocity. We assumed that the sound fields in the  $y$ -direction were uniform in this study. Equations (8) and (9) are derived from Eq. (7):

$$\dot{u} = \frac{\partial \Phi}{\partial x} - \frac{\partial \Psi}{\partial z}, \quad (8)$$

$$\dot{w} = \frac{\partial \Phi}{\partial z} + \frac{\partial \Psi}{\partial x}, \quad (9)$$

where  $\Psi$  is replaced by  $\Psi_2$ .

The following potential equations are obtained from Eqs. (5), (6), (8), and (9)

$$\rho \frac{\partial \dot{\Phi}}{\partial t} = c_{11} \left( \frac{\partial \dot{u}}{\partial x} + \frac{\partial \dot{w}}{\partial z} \right), \quad (10)$$

$$\rho \frac{\partial \dot{\Psi}}{\partial t} = c_{55} \left( \frac{\partial \dot{w}}{\partial x} - \frac{\partial \dot{u}}{\partial z} \right), \quad (11)$$

where  $\dot{\Phi}$  is  $\partial \Phi / \partial t$  and  $\dot{\Psi}$  is  $\partial \Psi / \partial t$ .  $\rho \dot{\Phi}$  and  $\rho \dot{\Psi}$  in Eqs. (10) and (11) have the units of stress.<sup>(9–11)</sup> The values of  $\rho \dot{\Phi}$  and  $\rho \dot{\Psi}$  describe the longitudinal and shear waves, respectively. The advantages of applying the velocity potential to the propagation of elastic waves are as follows.<sup>(9–11,13)</sup>

(1) Calculation load is minimized because the velocity potential is scalar.

(2) Longitudinal and shear waves can be independently examined by using  $\rho\dot{\Phi}$  and  $\rho\dot{\Psi}$ .

The elastic-wave equations used to examine the acoustic fields in the die and workpiece were solved by the FDTD method,<sup>(7–10)</sup> which can be used to simultaneously analyze the reflected and transmitted waves. The elastic wave equations were developed into difference equations in the spatial and time domains by the FDTD method.

The models used for calculating the acoustic fields on the basis of FDTD are shown in Fig. 9. The calculation model was developed to imitate the cylindrical stamping dies. The distance between the sound source and the workpiece at the center of the model is 20 mm. It was assumed that the workpiece and dies have a continuous contact surface and only their material properties differed. We used an aluminum thin plate as the workpiece, and the workpieces were 0.5 mm thick. The material properties of the workpieces and dies used in the analysis are listed in Table 1, where  $c_l$  and  $c_s$  are the wave velocities of the longitudinal and shear waves, respectively. All materials are isotropic.

In Fig. 9(a), points A and B are the observation points of the reflected and transmitted waves, respectively. The time step used in the FDTD method ( $\Delta t$ ) was 2 ns, and the spatial lattice interval was  $\Delta x = \Delta z = 20 \mu\text{m}$ . A sound source was placed at the bottom center of the calculation model and activated using the Gaussian pulse shown in Fig. 5. The frequency of the

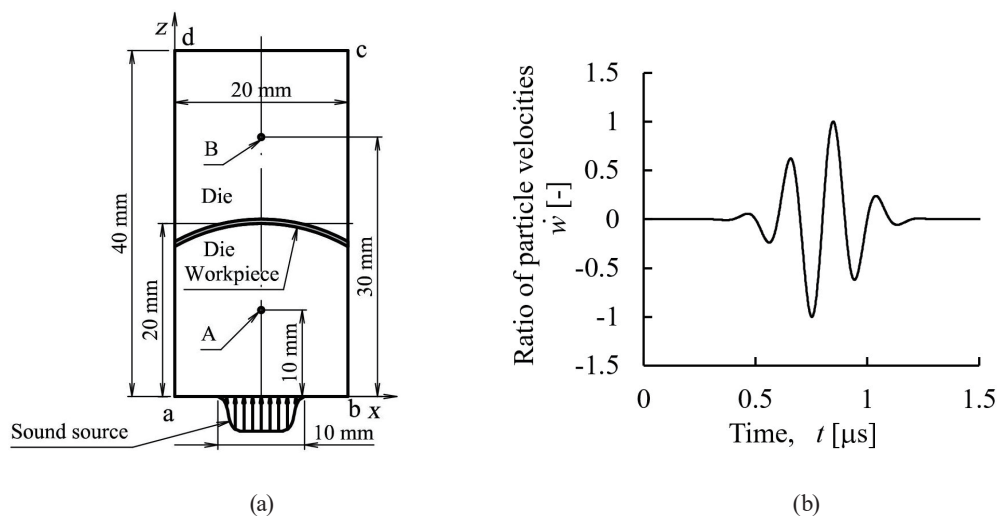


Fig. 9. Calculation model for propagation of elastic waves around the boundary surfaces of workpieces and cylindrical dies. (a) Analysis model. (b) Input wave (Gaussian pulse).

Table 1

Materials used in the numerical analysis of the acoustic field around the workpiece and stamping dies.

Material	Longitudinal elastic modulus	Density	Poisson's ratio	Wave velocity	
	$E$ (GPa)	$\rho$ ( $\text{kg}/\text{m}^3$ )	$\nu$ (-)	$c_l$ (m/s)	$c_s$ (m/s)
Steel (dies)	206	7850	0.29	5864	3189
Aluminum (workpiece)	70	2960	0.33	5919	2982

incident wave was 5 MHz. The boundary a–b of the calculation model was free, and the other boundaries (b–c, c–d, and c–a) were the absorbing boundaries. Mur's first-order absorbing conditions were applied as the absorbing boundary<sup>(13)</sup> to prevent unnecessary reflection of waves.

Acoustic fields were solved using the vector potential. Figure 10 shows the numerical results of calculation using the potential equations. The ratio of scalar velocity potential stress  $P_L$  in these figures is defined as

$$P_L = (\rho\dot{\Phi}) / (\rho\dot{\Phi}_0), \quad (12)$$

where  $\rho\dot{\Phi}_0$  is the maximum value of  $\rho\dot{\Phi}$  in the incident wave. The ultrasonic sensor used in the experiment can mainly detect only the longitudinal wave component.  $P_L$  describes the component of longitudinal waves. Therefore, the propagation of longitudinal waves can be examined by using  $P_L$ .

We examined the scalar velocity potential stress ratio distribution of the longitudinal wave component. The numerical results are shown in Fig. 10. The incident wave is either a transmitted wave or a reflected wave at the contact surface, as shown in Fig. 10(b). The transmitted longitudinal waves have a shape similar to that of the incident waves, and their amplitude is slightly smaller than that of the incident waves, but the transmitted waves are not greatly affected by the contact surface. The reflected waves deform after reflection at the contact surface Fig. 10(b). As shown in Fig. 10(c), the reflected waves are concentrated at one point owing to the effect of the cylindrical die surface, because the incident angle of an incident wave to the contact surface continuously varies along the contact surface. When the die radius

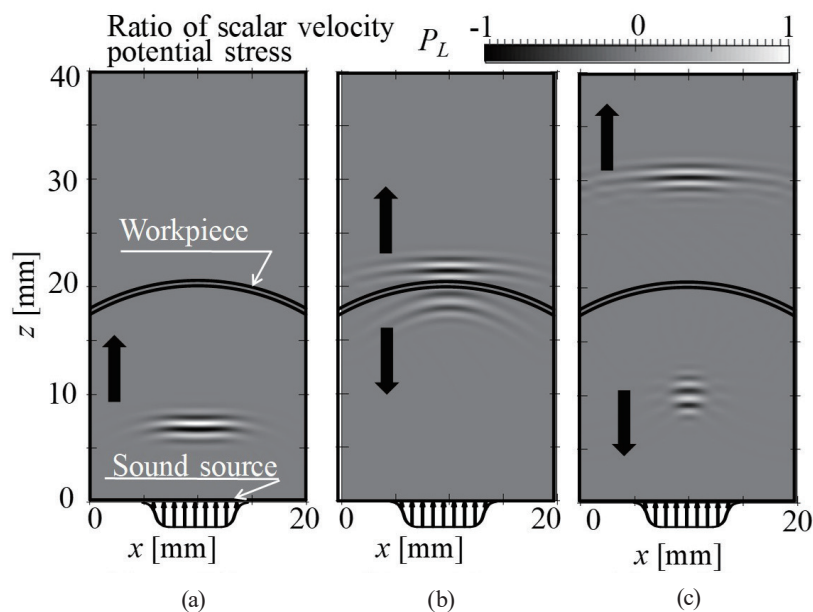


Fig. 10. Distribution of ratio of scalar velocity potential stress around boundary between surfaces of workpiece and cylindrical dies ( $R = 20$  mm,  $h = 0.5$  mm).<sup>(11)</sup> (a)  $t = 2.0$   $\mu$ s, (b)  $t = 4.5$   $\mu$ s, and (c)  $t = 6.0$   $\mu$ s.

was  $R = 20$  mm, the focal point of the reflected waves was about  $z = 8$  mm. Beyond the focal point, the reflected waves spread and their amplitude decreases. Furthermore, the effect of the radius of the cylindrical die on the amplitude of the transmitted/reflected waves was investigated. The results are shown in Figs. 11 and 12. In these figures,  $A_{LR}$  and  $A_{LT}$  are the reflected/transmitted wave amplitude ratios, which are defined as

$$A_{LR} = P_{L,R} / P_{L,0}, \quad (13)$$

$$A_{LT} = P_{L,T} / P_{L,0}, \quad (14)$$

where  $P_{L,0}$  is the maximum amplitude of the incident wave, and  $P_{L,R}$  and  $P_{L,T}$  are the amplitudes of the reflected and transmitted longitudinal waves, respectively.

Figure 11 shows the transmitted wave passing through point A in the calculation model in Fig. 9(a). The characteristics of the reflected ultrasonic waves are greatly affected by the die radius. The incident angle of the incident wave to the contact surface continuously varies along the contact surface, as shown in Fig. 8. If the receiver of the reflected wave is installed in the vicinity of the focal spot, the amplified wave can be measured. Thus, by numerical simulation, it can be verified whether the amplified wave can be measured.

Figure 12 shows the maximum amplitude of the scalar velocity potential ratio of the reflected wave passing through point B in Fig. 9(a). The maximum amplitude of the transmitted longitudinal wave is less affected by the die radius and is almost the same as that in the case of the flat dies. The analysis result indicates the same trend as the experiment result. As mentioned in the previous section, the transmitted waves were less affected by the die radius. We believe that the transmitted wave is refracted at both contact surfaces, and the propagation direction of the transmitted wave is almost the same as that of the incident wave. Therefore, if the transmitted wave is used, the contact state can be measured without being affected by the die shape. We believe that it is possible to determine the appropriate sensor position by propagation analysis for ultrasonic waves, which is based on the FDTD method.

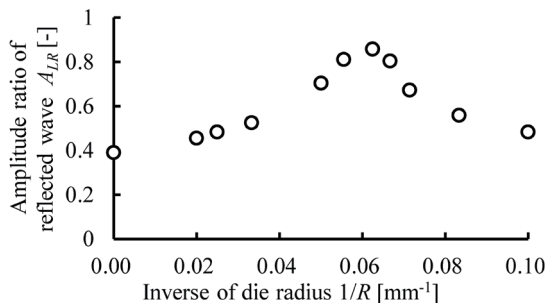


Fig. 11. Effect of die radius on reflection characteristics.

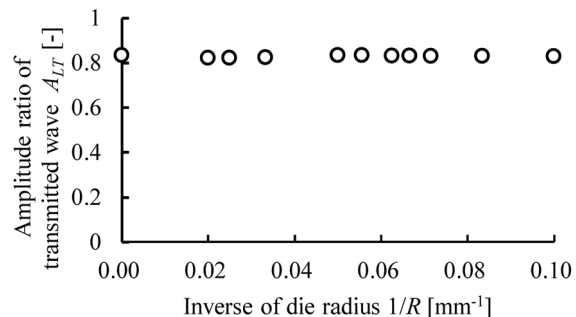


Fig. 12. Effect of die radius on transmission characteristics.

## 6. Conclusions

We have developed a method of using ultrasonic waves to measure the contact state between the workpiece and the cylindrical stamping die. We found that (1) the reflection of ultrasonic waves is affected by the shape of the die and (2) when a thin metal plate is firmly attached to the stamping die, the transmitted waves are not greatly affected by the shape of the die. If the press slide is controlled by feeding back the contact information obtained by this method to the servo press, gap can be expected to be removed. Also, it is possible to track the temporal change of deformation by measuring in-process. We believe that this method can be applied to not only stamping but also other plastic forming methods. We think that it is effective for detecting unfilled defects in die forging especially. Expansion of the application of this method would be expected in the verification of material flow during forging.

## Acknowledgments

This study was supported by the Amada Foundation, Japan, which the authors gratefully acknowledge.

## References

- 1 M. Masuko and Y. Ito: *Ann. CIRP XVII* (3) (1968) 289.
- 2 A. Takeuchi, Y. Kimura, T. Wakabayashi, T. Ishimaru, and H. Mori: *Trans. JSME Series C* **69** (2003) 3086 (in Japanese). <https://doi.org/10.1299/kikaic.69.3086>
- 3 A. Takeuchi, M. Satoh, M. Onozawa, Y. Sugawara, and H. Aoki: *Trans. JSME Series C* **65** (1999) 4767 (in Japanese). <https://doi.org/10.1299/kikaic.65.4767>
- 4 N. Hagino, J. Endou, S. Katoh, S. Okudera, M. Maruyama, M. Kubota, and C. Murata: *Steel Res. Int.* **81** (2010) 674. <https://doi.org/10.1002/srin.201190002>
- 5 N. Hagino, J. Endou, S. Katoh, S. Okudera, M. Maruyama, and M. Kubota: *Steel Res. Int. Special Ed.* **2011** (2011) 390.
- 6 N. Hagino, J. Endou, S. Katoh, and M. Ishihama: *Steel Res. Int. Special Ed.* **2012** (2012) 319.
- 7 N. Hagino, J. Endou, S. Katoh, and M. Ishihama: *Procedia Eng.* **81** (2014) 1073. <https://doi.org/10.1016/j.proeng.2014.10.143>
- 8 N. Hagino, S. Komiya, and M. Ishihama: *Proc. IN-TECH 2015* (2015) 1073–1078.
- 9 N. Hagino, S. Komiya, J. Endou, and M. Ishihama: *Key Eng. Mater.* **716** (2016) 528. <https://doi.org/10.4028/www.scientific.net/KEM.716.528>
- 10 N. Hagino, S. Komiya, J. Endou, and M. Ishihama: *Jpn. Soc. Technol. Plast.* **58** (2017) 929 (in Japanese). <https://doi.org/10.9773/sosei.58.929>
- 11 M. Sato: *Acoust. Sci. Technol.* **24** (2003) 415. <https://doi.org/10.1250/ast.24.415>
- 12 Y. Yamamoto: *Ultrasonic Wave Basics Engineering* (Nikkan Kogyo Shimbun Ltd., Tokyo, 1981).
- 13 T. Kimura, K. Misu, S. Wadaka, and M. Koike: *IEICE Technical Report* **105** (2006) 11 (in Japanese).

## About the Authors



**Naoto Hagino** received his B.S. degree in mechanical engineering from Kanagawa Institute of Technology, Japan, in 1993 and his M.S. and Ph.D. degrees from Kanagawa Institute of Technology, Japan, in 1995 and 2006, respectively. From 2006 to 2018, he was a part-time lecturer at Kanagawa Institute of Technology, Japan. Since 2018, he has been an associate professor at Kindai University Technical College. His research interests are in metal forming, turbomachinery, and thermal engineering. (hagino@kct.ac.jp)



**Seiji Komiya** received his B.S. degree in mechanical engineering from Yokohama National University, Japan, in 1988 and his M.S. degree from Yokohama National University, Japan, in 1990. From 1990 to 2018, he was an assistant professor at Kanagawa Institute of Technology, Japan. His research interests are in metal forming, automatic control, and mechanical engineering. (kom@eng.kanagawa-it.ac.jp)



**Junichi Endou** received his B.S. and M.S. degrees in mechanical engineering from Waseda University, Japan, in 1964 and 1966, respectively, and his Ph.D. degree from Tokyo Institute of Technology (TIT), Japan, in 1984. From 1966 to 1986, he was a research associate and then an associate professor at TIT, Japan. From 1986 to 1992, he was the general manager at the technical laboratory in AMADA Co., Ltd. In 1992, he became a professor at Kanagawa Institute of Technology, Japan, where he is now a professor emeritus. His research interests are in metal forming, especially tube bending, manufacturing systems, and sensing of sheet metal forming. (endo@sd.kanagawa-it.ac.jp)



**Masao Ishihama** received his B.S. degree in mechanical engineering from the University of Tokyo in 1969 and Ph.D. degree from Tokyo Institute of Technology, in 1996. From 1969 to 1997, he developed various new products at Nissan Motor Research Center. From 1997 to 2017, he was a professor at Kanagawa Institute of Technology. Since 2017, he has been a visiting professor at Kanagawa University. His research interests are in product design and NVH control. (ishihama@alum.mit.edu)